https://doi.org/10.5607/en22016
Exp Neurobiol. 2022 Jun;31(3):158-172.
pISSN 1226-2560 • eISSN 2093-8144

Original Article

Experimental Neurobiology

Generation of Astrocyte-Specific MAOB Conditional Knockout Mouse with Minimal Tonic GABA Inhibition

Jung Moo Lee[1,2†], Moonsun Sa[1,2†], Heeyoung An[2], Jong Min Joseph Kim[3], Jea Kwon[2], Bo-Eun Yoon[3] and C. Justin Lee[1,2*]

[1]KU-KIST Graduate School of Converging Science and Technology, Korea University, Seoul 02841, [2]Center for Cognition and Sociality, Institute for Basic Science, Daejeon 34126, [3]Department of Molecular biology, Dankook University, Cheonan 31116, Korea

Monoamine oxidase B (MAOB) is a key enzyme for GABA production in astrocytes in several brain regions. To date, the role of astrocytic MAOB has been studied in MAOB null knockout (KO) mice, although MAOB is expressed throughout the body. Therefore, there has been a need for genetically engineered mice in which only astrocytic MAOB is targeted. Here, we generated an astrocyte-specific MAOB conditional KO (cKO) mouse line and characterized it in the cerebellar and striatal regions of the brain. Using the CRISPR-Cas9 gene-editing technique, we generated *Maob* floxed mice (B6-*Maob*^{em1Cjl}/Ibs) which have floxed exons 2 and 3 of *Maob* with two loxP sites. By crossing these mice with hGFAP-CreER^{T2}, we obtained *Maob* floxed::hGFAP-CreER^{T2} mice which have a property of tamoxifen-inducible ablation of *Maob* under the human GFAP (hGFAP) promoter. When we treated *Maob* floxed::hGFAP-CreER^{T2} mice with tamoxifen for 5 consecutive days, MAOB and GABA immunoreactivity were significantly reduced in striatal astrocytes as well as in Bergmann glia and lamellar astrocytes in the cerebellum, compared to sunflower oil-injected control mice. Moreover, astrocyte-specific MAOB cKO led to a 74.6% reduction in tonic GABA currents from granule cells and a 76.8% reduction from medium spiny neurons. Our results validate that astrocytic MAOB is a critical enzyme for the synthesis of GABA in astrocytes. We propose that this new mouse line could be widely used in studies of various brain diseases to elucidate the pathological role of astrocytic MAOB in the future.

Key words: Astrocyte, MAOB, GABA, Striatum, Cerebellum, Conditional knockout mouse

INTRODUCTION

Monoamine oxidase B (MAOB), encoded by *Maob* on the X chromosome, is located in the outer membrane of mitochondria and metabolizes amines in the central nervous system and peripheral tissues [1]. MAOB is expressed throughout the brain, including the cerebellum, striatum, hippocampus, midbrain, and cerebral cortex [2-4]. At the cellular level, MAOB is mostly expressed in astrocytes and serotonergic neurons [5-8]. Especially, astrocytic MAOB is responsible for synthesizing GABA in the cerebellum [9, 10] and striatum [8, 9] under physiological conditions. Astrocytic GABA can be released from astrocytes via GABA-permeable Bestrophin-1 (Best1) channel leading to tonic inhibition of neighboring neurons [10, 11]. Interestingly, MAOB expression is elevated in several pathological conditions, such as Alzheimer's disease [12, 13], Parkinson's disease [14, 15], stroke [16], stab wound injury [17], obesity [18], and Huntington's disease [19], with the appearance of reactive astrocytes. Lines of evidence have described this pathological role of MAOB as responsible for aberrant tonic GABA synthesis in astrocytes [8, 12, 17]. Although MAOB is expressed not only in the brain but also in the peripheral tissues, MAOB null KO mice have been used to study the role of astrocytic MAOB [9, 15]. Therefore, there is a need for generating genetically engineered

Submitted April 28, 2022, Revised May 20, 2022, Accepted May 20, 2022

*To whom correspondence should be addressed.
TEL: 82-42-878-9150, FAX: 82-42-878-9151
e-mail: cjl@ibs.re.kr
†These authors contributed equally to this article.

mice that target only astrocytic MAOB.

For conditional KO of gene of interest in a mouse model, generation of floxed mice with loxP sites flanking the targeted exons is needed. Two major gene editing technologies are used to generate floxed mice: embryonic stem (ES) cell targeting and CRISPR-Cas9. The advent of ES cell-based gene targeting has resulted in advances in the field of neuroscience [20]. However, this technology is time-consuming and requires expensive equipment and technical skills such as micromanipulation and microinjection techniques [20, 21]. The most conspicuous disadvantage of ES cell targeting is its low success rate [22]. After CRISPR-Cas9 gene editing technology was adjusted for the engineering of mouse models [23, 24], it has been used extensively in the generation of floxed mice. CRISPR-Cas9 gene editing technology is about three times faster and about 30% cheaper than the ES cell targeting process [22]. The most important advantage of using the CRISPR-Cas9 approach is significantly higher efficiency of 85~95% success rate, compared to 50~55% success rate of ES cell targeting [22]. Therefore, we employed CRISPR-Cas9 to generate *Maob* floxed mice.

For astrocyte-specific manipulation and temporal control of the targeted gene, a mouse line with tamoxifen-inducible CreER^{T2} (Cre recombinase with estrogen receptor T2) expression under the astrocyte promoter is required, such as hGFAP-CreER^{T2} [25, 26] and Aldh1l1-Cre/ER^{T2} [27] mouse line. Although the mouse Aldh1l1 promoter has higher astrocyte specificity in the brain region than does the human GFAP promoter [25, 27], its application in a brain-specific manner is limited due to the high expression of *Aldh1l1* mRNA in other parts of the body [28]. Because MAOB is expressed throughout the body, hGFAP-CreER^{T2} mouse line would be more suitable for generating astrocyte-specific MAOB cKO mice than Aldh1l1-Cre/ER^{T2}. Therefore, we crossed *Maob* floxed mice with hGFAP-CreER^{T2} to generate astrocyte-specific MAOB cKO mice.

In this study, we generated new *Maob* floxed mice (B6-*Maob*^{em1Cjl}/Ibs) using the CRISPR-Cas9 gene editing technique, and further produced astrocyte-specific MAOB cKO mice by crossing *Maob* floxed mice with hGFAP-CreER^{T2} (B6-Tg(GFAP-cre/ERT2)13Kdmc). We investigated MAOB and GABA expression and tonic GABA release in cerebellar and striatal astrocytes by performing immunohistochemistry and slice patch-clamp recording in astrocyte-specific MAOB cKO mice. Consistent with previous studies on MAOB null KO mice, we validated that astrocyte-specific MAOB cKO mice showed minimal tonic GABA inhibition in the cerebellum and striatum.

MATERIALS AND METHODS

Animals

Mice were given *ad libitum* access to food and water, maintained under a 12:12 hour light-dark cycle, and housed in groups of 3~5 per cage. All mice were maintained on C57BL/6J strain. All care and handling of mice were conducted according to protocols approved by the directives of Institute for Basic Science (Daejeon, Republic of Korea).

Generation of Maob floxed mouse line

We requested the generation of *Maob* floxed mouse line to the Cyagen Biosciences (Guangzhou, China). Using CRISPR-Cas9 gene editing technique, *Maob* floxed allele was constructed. Two guide RNAs (gRNAs), which can be bound to 424 base pairs (bp) upstream of exon 2 and 429 bp downstream of exon 3, were designed with the following spacer sequences: spacer of gRNA1, 5'-TAAATACTATGTACTCTTAT-3'; spacer of gRNA2: 5'-CACAGAGAAAGCGCCCCTA-3'. Each of protospacer adjacent motif (PAM), AGG, for corresponding gRNA was located on the 3 bp downstream of each targeted DNA sequences. A cocktail of two gRNAs, donor vector containing loxP sites flanking the targeted exons along with 5' and 3' homology arms, and Cas9 nuclease mRNA was co-injected into fertilized mouse eggs. After each gRNA made a complex with Cas9 nuclease and was bound to the targeted DNA sequences in *Maob*, Cas9 nuclease recognized the PAM and caused the double-strand break at 3 bp upstream of PAM. Then, homology-directed recombination (HDR) between broken DNA and donor vector occurred as double-strand break repair mechanism. Finally, *Maob* floxed mice had *Maob* floxed allele which contained two loxP sites in upstream of exon 2 and downstream of exon 3. *Maob* floxed mice were maintained by crossing female heterozygous *Maob* floxed mice (X'X) with male wildtype (WT) mice. According to the nomenclature guideline for genetically engineered mouse established by the International Committee on Standardized Genetic Nomenclature for Mice, *Maob* floxed mouse line was named as B6-*Maob*^{em1Cjl}/Ibs.

Generation of astrocyte-specific MAOB cKO mouse line

Female heterozygous *Maob* floxed mice (B6-*Maob*^{em1Cjl}/Ibs, X'X) were crossed with male transgenic hGFAP-CreER^{T2} (B6-Tg(GFAP-cre/ERT2)13Kdmc, XY, TG) mice to generate male *Maob* floxed::hGFAP-CreER^{T2} (X'Y, TG) mice. Adult (aged 8~10 weeks) *Maob* floxed::hGFAP-CreER^{T2} (X'Y, TG) mice were treated with the tamoxifen at 100 mg/kg once per day for 5 days by intraperitoneal injection to generate the astrocyte-specific MAOB cKO mice. Tamoxifen was dissolved in sunflower oil containing

10% ethanol at concentration of 20 mg/ml. For control mice, same amount of sunflower oil was injected to the adult *Maob* floxed::hGFAP-CreER^{T2} (X'Y, TG) mice. Two or three weeks after injection, all mice were sacrificed for immunohistochemistry or tonic GABA slice recording.

Genotyping

Digestion of mouse tails was performed overnight at 60℃ using 1 mg/ml proteinase K (21560025-2, bioWORLD, USA) in tail lysis buffer (102-T, Viagenbiotech, USA). On the following day, proteinase K was inactivated for 1 hour at 85℃. The supernatant containing genomic DNA was used for genotyping. The PCR reaction mixture contained 2X PCR premix reagent (QM13531, Bioquest, Republic of Korea), 1 μl of genomic DNA template, 0.5 μM primer sets, and distilled water (DW). For *Maob* floxed mice, genotypes were determined by PCR using the following two pairs of primers to target each upstream and downstream loxP sites.

Pair 1: Forward #1 (F1), 5'-ATTCAGATTCACGGTCTGTGTTCA-3'
Reverse #1 (R1), 5'-ATGAAGAAGCAATGTGGAAGAGAG-3'
Pair 2: Forward #2 (F2), 5'-ATAGCTGACACCCTATTAACCCAC-3'
Reverse #2 (R2), 5'-CAAAGTGAGAATTCTGGGAAAGCA-3'

PCR using F1 and R1 primers for *Maob* floxed mice was performed with the following PCR cycling conditions: 94℃ for 3 min, 30 cycles of 94℃ for 30 s, 60℃ for 35 s, and 72℃ for 35 s, with the final elongation step at 72℃ for 5 min. PCR using F2 and R2 primers for *Maob* floxed mice was performed with the following PCR cycling conditions: 94℃ for 3 min, 35 cycles of 94℃ for 30 s, 60℃ for 35 s, and 72℃ for 35 s, with the final elongation step at 72℃ for 5 min. For GFAP-CreER^{T2} mice, genotypes were determined by PCR using the following two pairs of primers to target each hGFAP promoter and CreER^{T2} transgene based on previous report [25].

Pair 1: hGFAP forward, 5'-AGACCCATGGTCTGGCTCCAGGTAC-3'
BAC reverse, 5'-ATCGCTCACAGGATCACTCAC-3'
Pair 2: BAC forward, 5'-ACTGACATTTCTCTTGTCTCCTC-3'
CreER^{T2} reverse, 5'-TCCCTGAACATGTCCATCAGGTTC-3'

PCR was performed using both two pairs of primers at one time with the following PCR cycling conditions: 95℃ for 5 min, 35 cycles of 95℃ for 30 s, 58℃ for 30 s, and 72℃ for 30 s, with the final elongation step at 72℃ for 4 min. The PCR reaction products were run on 1% agarose gels (HB0100500, E&S, Republic of Korea) in TAE buffer (40 mM Tris, pH 7.6 with 20 mM acetic acid and 1 mM EDTA) at 100 V for 20 min and visualized using a safe nucleic acid staining solution, RedSafe (21141, iNtRON Biotechnology, Republic of Korea).

Sanger sequencing for loxP sites

Upstream loxP site near the exon 2 was amplified by PCR using F1 and R1 primers with same protocol for genotyping. A 312 bp of DNA band on agarose gel was extracted using gel extraction kit (CMG0112, COSMO GENETECH, Republic of Korea). Sanger sequencing of extracted DNA was performed using F1 primer. The sequencing results showed a deletion, ΔTATAGGGTT, and an insertion, CCTCAGGGAGCTCCCTAGGACGTAAACGGCCACAAGTTCGA, at the immediate upstream of loxP sequences. Downstream loxP site near the exon 3 was amplified by PCR using F2 and R2 primers with same protocol for genotyping. A 204 bp of DNA band on agarose gel was extracted using gel extraction kit (CMG0112, COSMO GENETECH, Republic of Korea). Sanger sequencing of extracted DNA was performed using R2 primer. The sequencing results showed a deletion, ΔCTA, and an insertion, GTCAGACTGGTCCGAATCCACAATATT, at the immediate downstream of loxP sequences. These deletions and insertions occurred at intron regions and did not affect exonic sequences.

Immunohistochemistry

Immunohistochemistry was performed using a modified protocol from the previous reports [25, 29]. For the slice preparation, adult mice were anesthetized with 1~2% isoflurane and perfused with 0.1 M phosphate buffered saline (PBS) followed by 4% paraformaldehyde. Extracted mouse brains were postfixed in 4% paraformaldehyde at 4℃ overnight and transferred to 30% sucrose solution for cryoprotection at 4℃ for more than 24 hours. Both sagittal (for cerebellum) and coronal (for striatum) sections were sectioned with 30 μm thickness in cryostat microtome (CM1950, Leica, USA). For the slice immunostaining, sections were first incubated for 1 hour in a blocking solution containing 0.3% Triton X-100 (X100, Sigma-Aldrich), 2% donkey serum (GTX27475, Genetex, USA), and 2% goat serum (ab7481, Abcam, UK) in 0.1 M PBS. Then, sections were immunostained with suitable mixtures of primary antibodies (Mouse anti-MAOB, sc-515354, Santa Cruz Biotechnology, USA, 1:100; Chicken anti-GFAP, AB5541, Millipore, USA, 1:500; Rabbit anti-S100β, ab41548, Abcam, UK, 1:200; Guinea pig anti-GABA, AB175, Millipore, USA, 1:200) in a blocking solution at 4℃ overnight. After extensive washing with PBS, sections were incubated with corresponding fluorescent secondary antibodies for 2 hours and then washed three time with PBS. If needed, DAPI (62248, Thermo Fisher Scientific, USA; 1:1000) staining was performed. The secondary antibodies were pur-

https://doi.org/10.5607/en22016

chased from Jackson ImmunoResearch Laboratories (USA). Then, sections were mounted on polysine adhesion microscope slides (Thermo Fisher Scientific, USA) with a fluorescent mounting medium (S3023, Dako, Denmark) and dried. Finally, fluorescent images were obtained with a Zeiss LSM900 confocal microscope, and Z-stack images in 2-μm steps were processed for further analysis using Imaris 9 (Bitplane, UK) software and ImageJ program (NIH, USA). Super-resolution images were obtained by Zeiss Elyra 7 Lattice SIM (Structured illumination microscopy), and obtained images were rendered with SIM-processing by Zen black software (Carl Zeiss, Germany).

Image quantification

Fluorescent images from confocal microscopy were analyzed using the Imaris 9 (Bitplane, UK) and ImageJ program (NIH, USA). To measure MAOB and GABA immunoreactivity in GFAP- or S100β-positive cells, surface of GFAP or S100β-positive cell was reconstructed using Imaris 9, and the volume values of each region of interest (ROI) and the integrated density values of MAOB and GABA intensity in each ROI were collected and analyzed. For measurement of MAOB and GABA immunoreactivity in GFAP- or S100β-negative areas, GFAP-negative areas were selected as each ROI using ImageJ, and MAOB and GABA immunoreactivity in every ROI were measured from 8-bit images.

Slice recording for tonic GABA

Slice recording was performed using a modified protocol from the previous reports [9, 10]. Mice were deeply anesthetized with isoflurane and decapitated to remove the brain. The brain was quickly excised from the skull and sectioned in an ice-cold sucrose-based dissection solution (in mM): 212.5 sucrose, 5 KCl, 10 $MgSO_4$, 1.23 NaH_2PO_4, 26 $NaHCO_3$, 0.5 $CaCl_2$, 10 glucose, pH 7.4. After cerebellum region was chopped from the brain, 300 μm sagittal slices for cerebellum and horizontal slices from striatum were cut using a vibratome (DSK Linear Slicer, Japan). After slicing, slices transferred to extracellular artificial cerebrospinal fluid (ACSF) solution (in mM): 130 NaCl, 24 $NaHCO_3$, 1.25 NaH_2PO_4, 3.5 KCl, 1.5 $CaCl_2$, 1.5 $MgCl_2$, and 10 glucose, pH 7.4. Slices were incubated at room temperature for at least one hour prior to recording. The whole solution was gassed with 95% O_2 and 5% CO_2. For tonic GABA recording, whole-cell patch-clamp recordings were made from cerebellar granule cells located in lobules 2~5 and medium spiny neurons located in dorsal striatum. We used the holding potential of -70 mV for tonic GABA recording in medium spiny neurons by referring to our previous report [9]. Furthermore, we referred to our recent papers [10, 30] to record the tonic GABA in the granule cells and used the holding potential of -60 mV. Patch electrode (6~8 MΩ) was filled with an internal solution (in mM): 135 CsCl, 4 NaCl, 0.5 $CaCl_2$, 10 HEPES, 5 EGTA, 2 Mg-ATP, 0.5 Na_2-GTP, 10 QX-314, pH adjusted to 7.2 with CsOH (278~285 mOsmol/kg). Baseline current was stabilized under treatment of 50 μM D-AP5 (0106, Tocris), 20 μM CNQX (0190, Tocris). The amplitude of $GABA_A$ receptor mediated tonic GABA current was measured by the baseline shift after 50 μM Gabazine (GBZ; 1262, Tocris) application for recording in the cerebellum and 50 μM (-)-Bicuculine methobromide (Bic; 0109, Tocris) application for recording in the striatum. The negative values of tonic GABA current in the striatum were analyzed as zero. The amplitude of full activated GABA current was measured by the current shift between current after 5 or 10 μM GABA (A2129, Sigma-Aldrich) application and current after 5 or 10 μM GABA with 50 μM GBZ or 50 μM Bic application in the cerebellum or striatum, respectively. Electrical signals were amplified using MultiClamp 700B (Molecular Devices, USA). Data including membrane capacitance (Cm) was acquired by a Digitizer 1550B and pClamp 11 software (Molecular Devices, USA). Data were filtered at 2 kHz. Tonic current and full activated GABA current were analyzed by Clampfit software (Molecular Devices, USA). Frequency and amplitude of spontaneous IPSCs were analyzed by Minianalysis software (Synaptosoft).

Statistical analysis

For all experiments, data normality was analyzed using a D'Agostino-Pearson omnibus normality test. For data following normal distribution, differences between groups were evaluated by unpaired two-tailed t test or Welch's test. For data not following normal distribution, a Mann-Whitney test (Two-tailed) was performed. The significance level is represented as asterisks (*$p<0.05$; **$p<0.01$; ***$p<0.001$; ****$p<0.0001$; n.s., not significant). Outliers were excluded by Grubb's test or ROUT method. GraphPad Prism 9.3.1 for Windows (GraphPad Software, USA) was used for these analyses and to create the plots.

RESULTS

Generation of Maob floxed and astrocyte-specific MAOB cKO mouse lines

Maob of *Mus musculus* (NC_000086.8) is located on the reverse strand of X chromosome (XqA1.2), 16,575,520~16,683,605, and consists of 15 exons (Fig. 1A). To generate *Maob* floxed mice, a *Maob* floxed allele was constructed using CRISPR-Cas9 gene editing techniques. Two guide RNAs (gRNAs), which can be bound to 424 bp upstream of exon 2 and 429 bp downstream of exon 3, were designed (Fig. 1A). A cocktail containing two gRNAs, donor

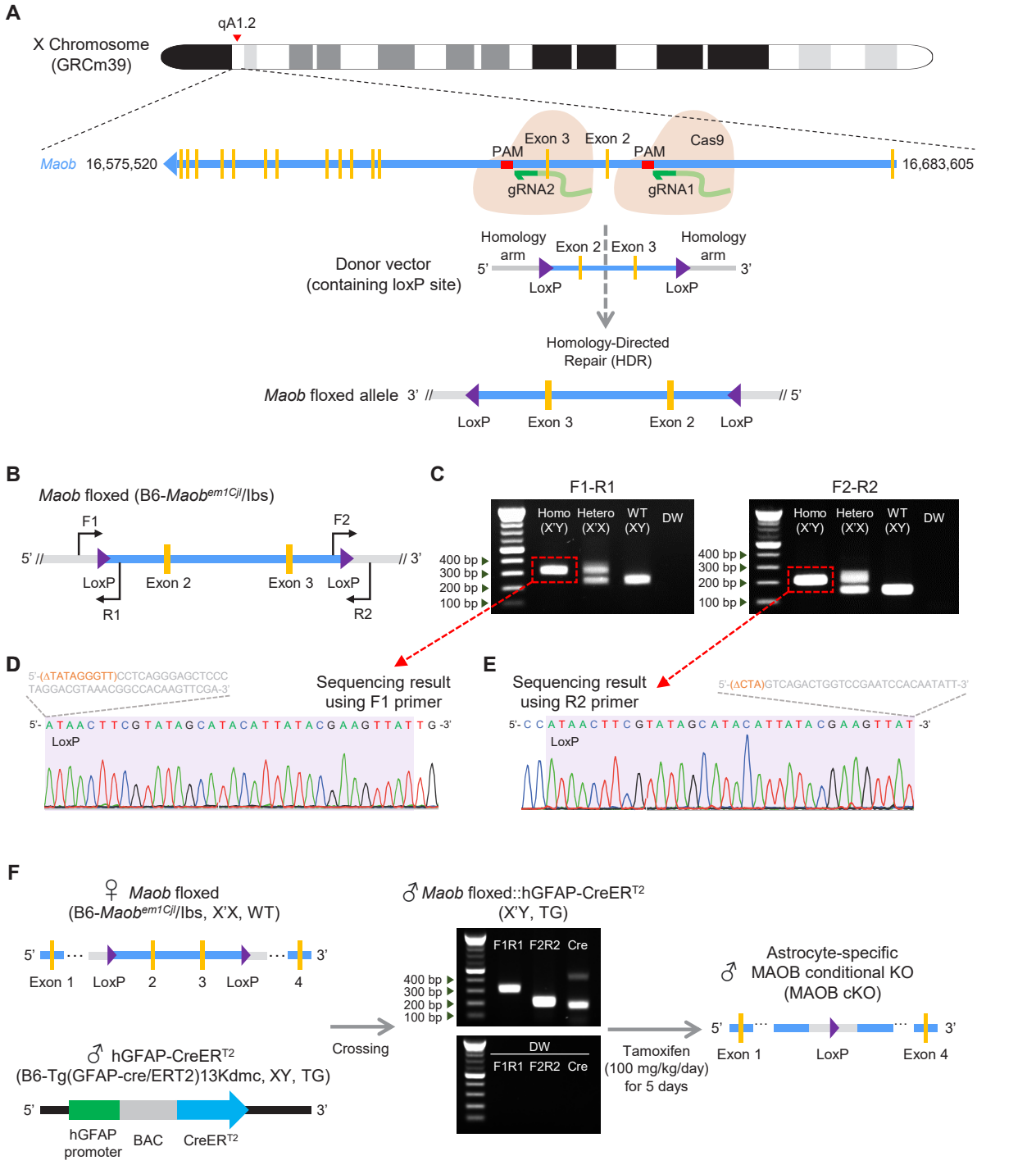

Fig. 1. Generation of *Maob* floxed and astrocyte-specific MAOB cKO mouse lines. (A) Schematic diagram of *Maob* location on mouse X chromosome (top) and construction of *Maob* floxed allele using the CRIPSR-Cas9 technique (bottom). (B) Construct of *Maob* floxed allele in *Maob* floxed mouse (B6-*Maob*^{em1Cjl}/Ibs) with primer sets for genotyping (F1-R1, F2-R2) and sequencing (F1, R2) for each loxP site. (C) Genotyping result of homozygote, heterozygote, WT, and distilled water (DW) as no template control using F1-R1 primer (left) and F2-R2 primer (right). Red dotted boxes and lines indicate extracted DNA bands for sequencing in (D) and (E). (D) Sequencing result of loxP site in upstream of exon 2 using F1 primer. Orange and grey sequences indicate deleted and inserted intronic sequences from the original *Maob*, respectively. (E) Sequencing result of loxP site in downstream of exon 2 using R2 primer. Orange and grey sequences indicate deleted and inserted intronic sequences from the original *Maob*, respectively. (F) Schematic diagram showing generation of astrocyte-specific MAOB cKO mice by crossing *Maob* floxed mice (B6-*Maob*^{em1Cjl}/Ibs, X'X, WT) with hGFAP-CreER^{T2} (B6-Tg(GFAP-cre/ERT2)13Kdmc, XY, TG) (left), and genotyping results of *Maob* floxed::hGFAP-CreER^{T2} (X'Y, TG) with F1-R1, F2-R2, and two pairs of primers for hGFAP-CreER^{T2} with no template control of each primer set (middle), and construct of *Maob* allele in astrocyte-specific MAOB cKO mouse (right).

https://doi.org/10.5607/en22016

vector, and Cas9 nuclease mRNA was co-injected into fertilized mouse eggs. After each gRNA formed a complex with Cas9 and was bound to targeted DNA sequences, Cas9 recognized the protospacer adjacent motif (PAM) and induced the DNA double-strand break. Then, the broken DNAs were repaired by homology-directed recombination (HDR) with the donor vector containing two loxP sites, targeted exons, and homology arms (Fig. 1A). Consequently, *Maob* floxed allele contained two loxP sites upstream of exon 2 and downstream of exon 3 (Fig. 1A).

We then genotyped *Maob* floxed mice (B6-*Maob*^{em1Cjl}/Ibs) using two sets of primers to detect the insertion of two loxP sites in the upstream region near exon 2 and in the downstream region near exon 3 (Fig. 1B). When we performed PCR using the forward #1 (F1) and reverse #1 (R1) primers to check loxP insertion in the upstream regions, *Maob* floxed allele produced a DNA band of 312 bp and WT allele produced a DNA band of 246 bp. We observed three genotypes in the mice: homozygote (homo) with one band of 312 bp, heterozygote (hetero) with two bands of 312 bp and 246 bp, and WT with one band of 246 bp (Fig. 1C). In addition to the upstream loxP site, we further genotyped mice using forward #2 (F2) and reverse #2 (R2) primers to detect loxP insertion in the downstream regions (Fig. 1B). We observed a 204 bp DNA band for *Maob* floxed allele and 146 bp DNA band for WT allele with three genotypes: homozygote (homo) with one band of 204 bp, heterozygote (hetero) with two bands of 204 bp and 146 bp, and WT with one band of 146 bp (Fig. 1C). Moreover, we found that both upstream and downstream loxP sequences were located at the targeted sites and had original 34 bp sequences without any mutation, by performing DNA sequencing for each band of the *Maob* floxed allele (Fig. 1D, E). However, there were inadvertent deletions and insertions immediately upstream or downstream of each loxP site (Fig. 1D, E). These deletions and insertions occurred at intron regions and did not affect exonic sequences.

Next, to generate astrocyte-specific MAOB cKO mice, *Maob* floxed mice were crossed with hGFAP-CreER^{T2} (B6-Tg(GFAP-cre/ERT2)13Kdmc), resulting in the production of *Maob* floxed:: hGFAP-CreER^{T2} mice. Since *Maob* is located on the X chromosome, female heterozygous *Maob* floxed mice (X'X for *Maob* floxed, WT for CreER^{T2}) and male transgenic (TG) hGFAP-creER^{T2} (XY for *Maob* floxed, TG for CreER^{T2}) were crossed to obtain male homozygous mice for *Maob* floxed (X'Y) with transgenic for CreER^{T2} (Fig. 1F). These mice were genotyped using the F1-R1 and F2-R2 primer sets for *Maob* floxed, and the protocol for hGFAP-CreER^{T2} based on our previous report [25]. Intraperitoneal injection of tamoxifen (100 mg/kg/day) for 5 consecutive days into the *Maob* floxed::hGFAP-CreER^{T2} (X'Y for *Maob* floxed, TG for CreER^{T2}) caused CreER^{T2} translocation to the nucleus, followed by excision of loxP-flanked exon 2 and 3 under the control of human GFAP promoter, resulting in the generation of astrocyte-specific MAOB cKO mice (Fig. 1F).

MAOB and GABA levels in the cerebellum are reduced in astrocyte-specific MAOB cKO mice

We have previously reported that cerebellar glial cells, such as Bergmann glia and lamellar astrocytes, express MAOB and contain GABA [9, 11]. Thus, we first examined whether MAOB and GABA levels can be reduced in cerebellar glia of astrocyte-specific MAOB cKO mice. To measure MAOB and GABA levels in the cerebellum, we injected 100 mg/kg tamoxifen for 5 consecutive days into *Maob* floxed::hGFAP-CreER^{T2} mice to induce astrocyte-specific MAOB ablation (Fig. 2A). After 2~3 weeks, we performed immunostaining of cerebellar sagittal slices with antibodies against MAOB and GFAP, an astrocyte marker, and obtained confocal microscopy images in the granule cell layer (GCL) and molecular layer (ML) of the cerebellum (Fig. 2B). As a result, the intensity of MAOB immunoreactivity in GFAP-positive cells was significantly decreased in the GCL and ML of tamoxifen-injected MAOB cKO mice, compared to MAOB control mice injected with sunflower oil (Fig. 2C, D). In contrast, MAOB immunoreactivity in GFAP-negative areas showed no difference between two groups (Fig. 2E, F). The immunostained cerebellar slices were also imaged using Lattice SIM to visualize MAOB in more detail at ultrastructural resolution. Consistent with the results of confocal microscopy, we observed that MAOB levels, shown as green dots, decreased in astrocyte-specific MAOB cKO mice (Fig. 2G). Moreover, we measured GABA levels in cerebellar astrocytes using antibodies against GABA and GFAP under confocal microscopy (Fig. 2H). We found significantly reduced GABA immunoreactivity in GFAP-positive cells in the GCL and ML of the astrocyte-specific MAOB KO mice (Fig. 2I, J), but not in GFAP-negative areas (Fig. 2K, L). Interestingly, there was a more striking reduction in astrocytic GABA content in the GCL than in the ML (Fig. 2I, J). These findings indicate that GABA in lamellar astrocytes in the GCL is mainly synthesized by MAOB, whereas GABA in Bergmann glia in the ML is partially synthesized by MAOB. Taken together, we validate that the newly generated astrocyte-specific MAOB cKO mice show a significant reduction in astrocytic MAOB expression and GABA content in the cerebellum.

Astrocyte-specific MAOB cKO mice show a significant reduction in tonic GABA inhibition in the cerebellum

We have previously demonstrated that MAOB null KO mice showed a significant reduction in tonic GABA release from granule cells in the cerebellum [9, 10]. Moreover, astrocyte-specific

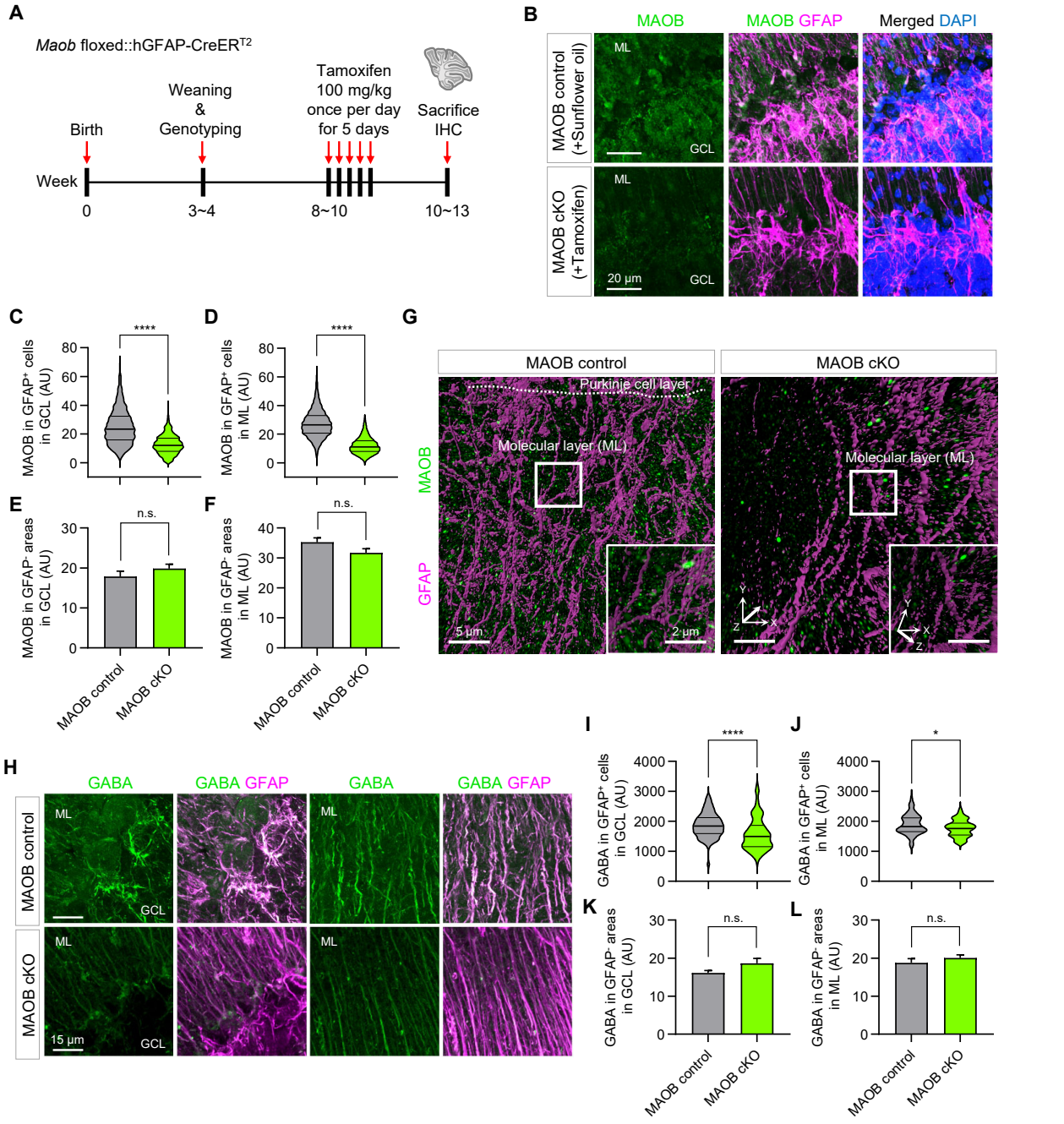

Fig. 2. MAOB and GABA levels in the cerebellum are reduced in astrocyte-specific MAOB cKO mice. (A) Experimental scheme and timeline using *Maob* floxed::hGFAP-CreER^{T2} mice. (B) Representative confocal images of MAOB (green), GFAP (magenta) and DAPI (blue) fluorescence in sagittal slices of the cerebellum in sunflower oil-injected MAOB control and tamoxifen-injected MAOB cKO mice. ML, molecular layer; GCL, granule cell layer. (C, D) Quantification of MAOB intensity in GFAP-positive cells in the GCL (C; MAOB control, 2186 voxels; MAOB cKO, 695 voxels; Mann-Whitney test, $p<0.0001$) and in the ML (D; MAOB control, 3455 voxels; MAOB cKO, 9916 voxels; Mann-Whitney test, $p<0.0001$). (E, F) Quantification of MAOB intensity in GFAP-negative areas in the GCL (E; MAOB control, 27 pixels; MAOB cKO, 22 pixels; Mann-Whitney test, $p=0.8034$) and in the ML (F; MAOB control, 22 pixels; MAOB cKO, 19 pixels; Mann-Whitney test, $p=0.1084$). (G) Representative SIM images of MAOB (green) and GFAP (magenta) in sagittal slices of cerebellum in MAOB control (left) and astrocytic MAOB cKO mice (right). White boxes, magnified regions. Insets, magnified and rotated 3-dimensional (3D) images. (H) Representative images for GABA (green) and GFAP (magenta) in sagittal slices of cerebellum in MAOB control and astrocytic MAOB cKO mice. (I, J) Quantification of GABA intensity in GFAP-positive cells in the GCL (I; MAOB control, 73 voxels; MAOB cKO, 84 voxels; Mann-Whitney test, $p<0.0001$) and in the ML (J; MAOB control, 68 voxels; MAOB cKO, 63 voxels; Unpaired t test, $p<0.05$). (K, L) Quantification of GABA intensity in GFAP-negative areas in the GCL (K; MAOB control, 20 pixels; MAOB cKO, 22 pixels; Mann-Whitney test, $p=0.1508$) and in the ML (L; MAOB control, 26 pixels; MAOB cKO, 33 pixels; Mann-Whitney test, $p=0.5119$). In violin plots, the center line denotes the median value, while upper and lower lines denote the first quartile and third quartile, respectively. Data are presented as mean±SEM. ****$p<0.0001$; *$p<0.05$; n.s., not significant.

https://doi.org/10.5607/en22016

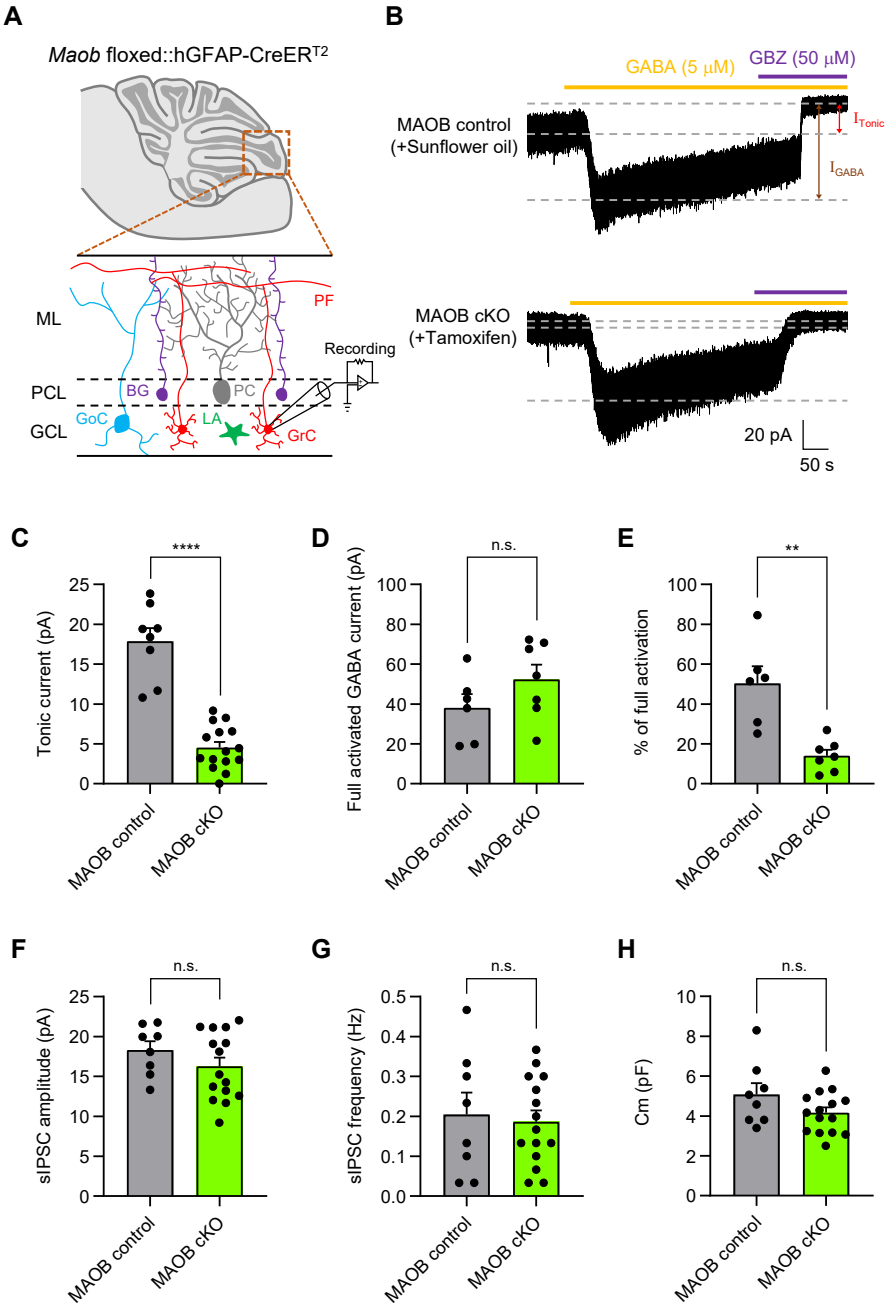

Fig. 3. Astrocyte-specific MAOB cKO mice show a significant reduction in tonic GABA inhibition in the cerebellum. (A) Schematic diagram of a cerebellar slice from *Maob* floxed::hGFAP-creER^{T2} mice (top) and magnified image of a whole-cell patch-clamped region in the cerebellar layers (bottom). GCL, Granule cell layer; PCL, Purkinje cell layer; ML, Molecular layer; Grc, Granule cell; GoC, Golgi cell; PC, Purkinje cell; BG, Bergmann glia; LA, Lamellar astrocyte; PF, Parallel fiber. (B) Representative tonic current traces from sunflower oil-injected MAOB control mice (top) and tamoxifen-injected MAOB cKO mice (bottom). Full activated GABA current (I_{GABA}, brown arrow) and ambient GABA current (I_{Tonic}, red arrow) were measured by serial application of GABA 5 μM (orange dash) and GBZ 50 μM (purple dash). (C) Summarized scatter bar graphs of tonic current from MAOB control mice and astrocytic MAOB cKO mice (MAOB control, n=8; MAOB cKO, n=15; Unpaired t test, p<0.0001). (D) Summarized scatter bar graphs of full activated GABA current (MAOB control, n=6; MAOB cKO, n=7; Mann-Whitney test, p=0.1807). (E) Summarized scatter bar graphs of percentage of full activation (I_{Tonic}/I_{GABA}) (MAOB control, n=6; MAOB cKO, n=7; Mann-Whitney test, p=0.0023). (F) Summarized scatter bar graphs of sIPSC amplitude (MAOB control, n=8; MAOB cKO, n=15; Unpaired t test, p=0.2423). (G) Summarized scatter bar graphs of sIPSC frequency (MAOB control, n=8; MAOB cKO, n=15; Unpaired t test, p=0.7551). (H) Summarized scatter bar graphs of cell membrane capacitance (Cm) (MAOB control, n=8; MAOB cKO, n=15; Unpaired t test, p=0.1125). Data are presented as mean±SEM. ****p<0.0001; **p<0.01; n.s., not significant.

rescue of *Maob* restored tonic GABA inhibition in the cerebellum [9]. Thus, we tested whether astrocyte-specific MAOB cKO mice show elimination of tonic inhibition in the cerebellum by recording tonic GABA currents from cerebellar granule cells (Fig. 3A), according to the same timeline as Fig. 2A. The $GABA_A$ receptor-mediated tonic currents were measured as a current shift during treatment with the $GABA_A$ receptor antagonist, Gabazine (GBZ; 50 μM) (Fig. 3B). The GBZ-sensitive tonic GABA current was significantly decreased by 74.6% in tamoxifen-injected MAOB cKO mice, compared to sunflower oil-injected MAOB control mice (Fig. 3C). This abolishment of the tonic GABA current was not due to altered extrasynaptic $GABA_A$ receptor expression, as evidenced by the absence of significant change in the 5 μM GABA-induced full activation current (Fig. 3D). Moreover, the percentage of full activation, calculated by dividing the tonic GABA current by the full GABA current, was significantly lower in astrocyte-specific MAOB cKO mice (Fig. 3E). These results indicate that MAOB in cerebellar astrocytes is required for tonic inhibition in the cerebellum. In contrast, we found no alteration in the amplitude and frequency of spontaneous inhibitory postsynaptic current (sIPSC) (Fig. 3F, G), indicating that synaptic GABA release was not changed in astrocyte-specific MAOB cKO mice. Furthermore, patched cells in each group had similar membrane capacitance (Cm) (Fig. 3H), suggesting that the reduction in tonic GABA current in astrocyte-specific MAOB cKO mice was not due to changes in neuronal cell size. Taken together, we confirm that the astrocyte-specific MAOB cKO mice exhibit a major reduction in tonic GABA inhibition in the cerebellum.

MAOB and GABA levels in the striatum are reduced in astrocyte-specific MAOB cKO mice

In addition to the cerebellum, tonic inhibition has been reported in the medium spiny neurons (MSNs) of the striatum [9, 31, 32]. Therefore, we investigated the MAOB and GABA levels in the striatum of MAOB control and astrocyte-specific MAOB cKO mice. To assess MAOB and GABA levels in the striatum, we injected tamoxifen and performed immunohistochemistry, according to the same timeline as in the experiment for the cerebellum (Fig. 4A). After 2~3 weeks of injection, we performed immunostaining of striatal coronal slices with antibodies against MAOB and S100β (Fig. 4B), instead of GFAP, because of the low expression of GFAP in striatal astrocytes [33]. Compared to sunflower oil-injected MAOB control mice, tamoxifen-injected MAOB cKO mice showed significantly reduced MAOB intensity in S100β-positive cells under confocal microscopy (Fig. 4C), but not in S100β-negative areas (Fig. 4D). Furthermore, we found that MAOB levels decreased in astrocyte-specific MAOB cKO mice from Lattice SIM images (Fig. 4E), consistent with the results of confocal microscopy. In addition to MAOB, we observed a significant reduction of GABA immunoreactivity in S100β-positive cells in the astrocyte-specific MAOB KO mice from confocal microscopy images (Fig. 4F, G), but not in S100β-negative areas (Fig. 4H). These results indicate that the newly generated astrocyte-specific MAOB cKO mice exhibit a significant reduction in astrocytic MAOB expression and GABA content in the striatum.

Astrocyte-specific MAOB cKO mice show a significant reduction in tonic GABA inhibition in the striatum

We have previously reported that tonic GABA release in the striatum can be decreased in the MAOB null KO mice [9]. Moreover, reduced tonic GABA currents from hGFAP-$CreER^{T2}$ mice injected with lentivirus carrying pSicoR-MAOB shRNA were restored by the rescue of astrocytic MAOB by treating tamoxifen [9]. Thus, we examined the contribution of astrocytic MAOB to $GABA_A$ receptor-mediated tonic currents in the striatal region of astrocyte-specific MAOB cKO mice using another $GABA_A$ receptor antagonist, bicuculline (Bic; 50 μM) (Fig. 5A, B). The Bic-sensitive tonic GABA current was significantly reduced by 76.8% in tamoxifen-injected MAOB cKO mice, compared to sunflower oil-injected MAOB control mice (Fig. 5C), while there was no significant change in 10 μM GABA-induced full activation current in either group (Fig. 5D). Moreover, the percentage of full activation in astrocyte-specific MAOB cKO mice was significantly lower than that in the MAOB control mice (Fig. 5E). In contrast, the $GABA_A$ receptor-mediated sIPSC amplitude, frequency, and membrane capacitance did not differ between astrocyte-specific MAOB cKO and MAOB control mice (Fig. 5F~H). Consequently, these results indicate that astrocyte-specific MAOB cKO mice show a major reduction in tonic GABA inhibition in the striatum.

DISCUSSION

We have successfully generated the *Maob* floxed mice (B6-*Maob*^{em1Cjl}/Ibs) using the CRISPR-Cas9 gene editing technique and crossed these mice with hGFAP-$CreER^{T2}$ to generate astrocyte-specific MAOB cKO mice. As expected, these mice showed minimal tonic GABA inhibition with reduced levels of MAOB expression and GABA content in astrocytes of the cerebellum and striatum (Fig. 6). Our study strengthens the established theory that astrocytic MAOB is critical for synthesizing GABA for tonic inhibition, independent of phasic inhibition. This new mouse model should prove to be useful for elucidating the role of astrocytic MAOB under various physiological and pathological conditions.

MAOB null KO mice have yielded limited understanding of the

https://doi.org/10.5607/en22016

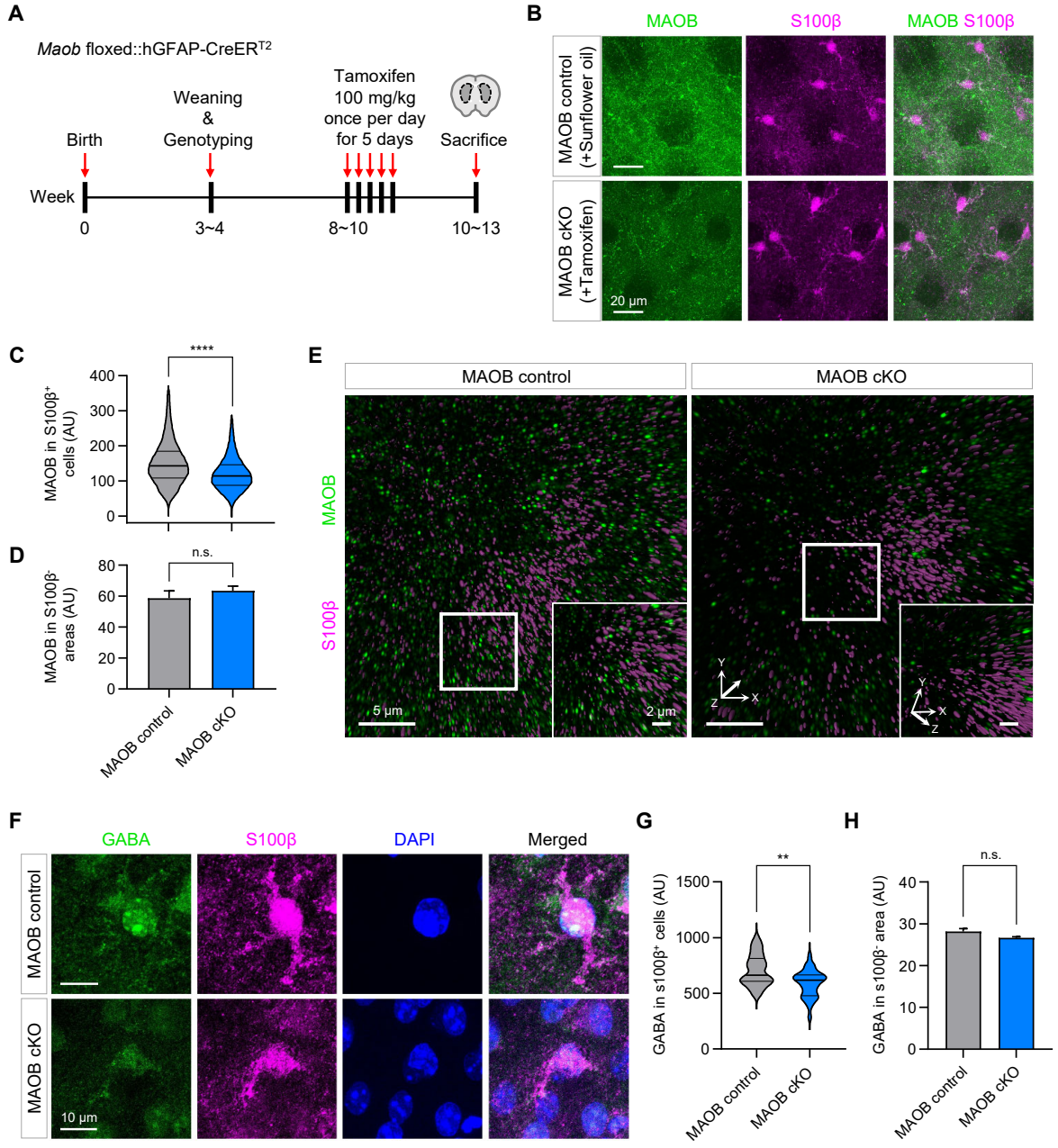

Fig. 4. MAOB and GABA levels in the striatum are reduced in astrocyte-specific MAOB cKO mice. (A) Experimental scheme and timeline using *Maob* floxed::hGFAP-CreER^{T2} mice. (B) Representative confocal images of MAOB (green), S100β (magenta) in coronal slices of striatum in sunflower oil-injected MAOB control and tamoxifen-injected MAOB cKO mice. (C) Quantification of MAOB intensity in S100β-positive cells in the striatum (MAOB control, 130316 voxels; MAOB cKO, 89368 voxels; Mann-Whitney test, p<0.0001). (D) Quantification of MAOB intensity in S100β-negative areas in the striatum (MAOB control, 75 pixels; MAOB cKO, 73 pixels; Mann-Whitney test, p=0.5655). (E) Representative SIM images of MAOB (green) and S100β (magenta) in coronal slices of striatum in MAOB control (left) and astrocytic MAOB cKO mice (right). White boxes, magnified regions. Insets, magnified and rotated 3D images. (F) Representative images for GABA (green), S100β (magenta) and DAPI (blue) in coronal slices of striatum in MAOB control and astrocytic MAOB cKO mice. (G) Quantification of GABA intensity in S100β-positive cells in the striatum (MAOB control, 28 voxels; MAOB cKO, 30 voxels; Unpaired t test, p<0.01. (H) Quantification of GABA intensity in S100β-negative areas in the striatum (MAOB control, 85 pixels; MAOB cKO, 75 pixels; Mann-Whitney test, p=0.1110). In violin plots, the center line denotes the median value, while upper and lower lines denote the first quartile and third quartile, respectively. Data are presented as mean±SEM. ****p<0.0001; **p<0.01; n.s., not significant.

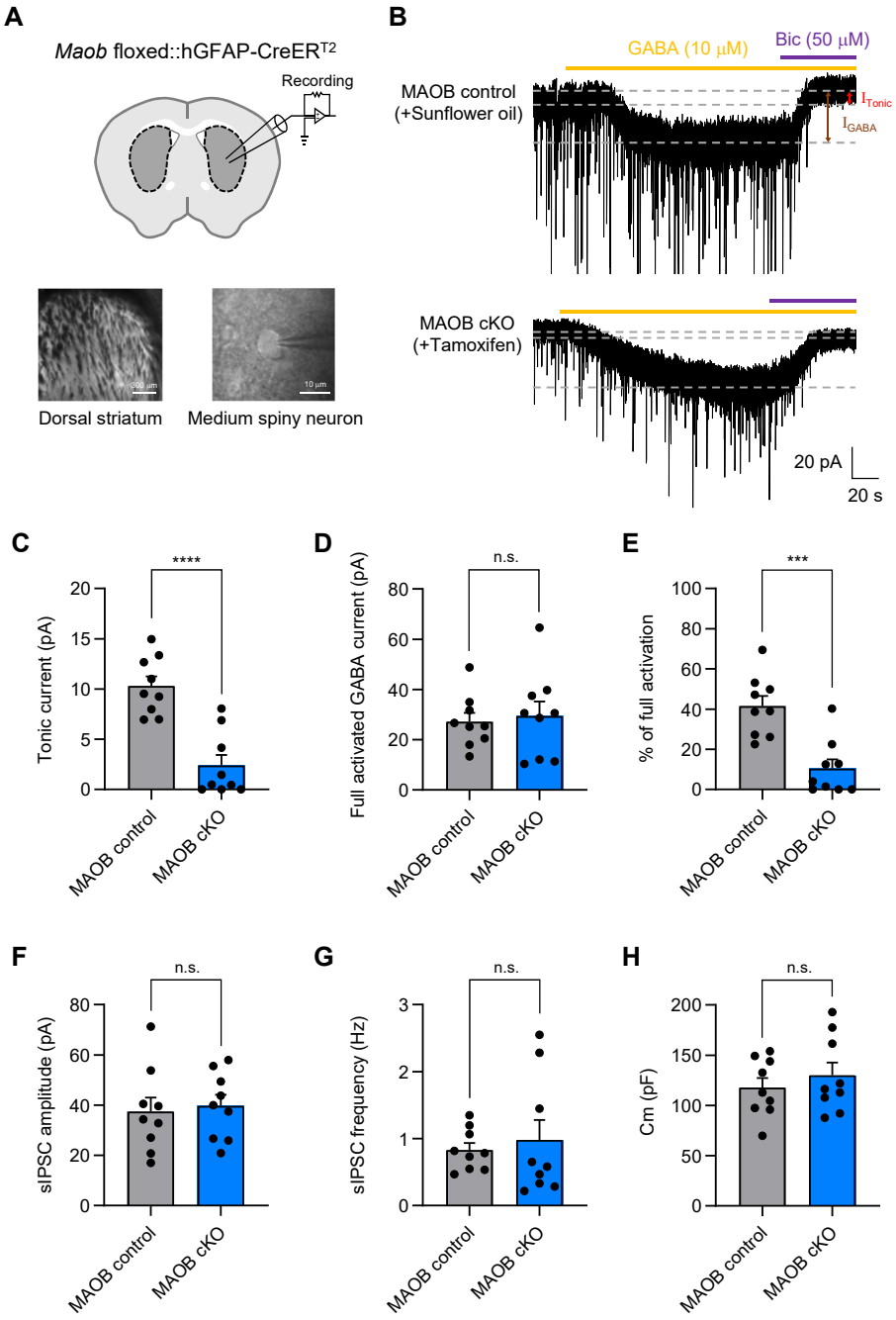

Fig. 5. Astrocyte-specific MAOB cKO mice show a significant reduction in tonic GABA inhibition in the striatum. (A) Schematic diagram of a striatal slice from *Maob* floxed::hGFAP-creER^{T2} mice (top) and magnified differential interference contrast (DIC) image of a whole-cell patch-clamped region in the dorsal striatum and medium spiny neurons (bottom). (B) Representative tonic current traces from sunflower oil-injected MAOB control mice (top) and tamoxifen-injected MAOB cKO mice (bottom). Full activated GABA current (I_{GABA}, brown arrow) and ambient GABA current (I_{Tonic}, red arrow) were measured by serial application of GABA 10 μM (orange dash) and Bic 50 μM (purple dash). (C) Summarized scatter bar graphs of tonic current from MAOB control mice and astrocytic MAOB cKO mice (MAOB control, n=9; MAOB cKO, n=9; Unpaired t test, p<0.0001). (D) Summarized scatter bar graphs of full activated GABA current (MAOB control, n=9; MAOB cKO, n=9; Unpaired t test, p=0.7359). (E) Summarized scatter bar graphs of percentage of full activation (I_{Tonic}/I_{GABA}) (MAOB control, n=9; MAOB cKO, n=9; Mann-Whitney test, p=0.0008). (F) Summarized scatter bar graphs of sIPSC amplitude (MAOB control, n=9; MAOB cKO, n=9; Unpaired t test, p=0.7534). (G) Summarized scatter bar graphs of sIPSC frequency (MAOB control, n=9; MAOB cKO, n=9; Welch's test, p=0.6530). (H) Summarized scatter bar graphs of cell membrane capacitance (Cm) (MAOB control, n=9; MAOB cKO, n=9; Unpaired t test, p=0.4500). Data are presented as mean±SEM. ****p<0.0001; ***p<0.001; n.s., not significant.

https://doi.org/10.5607/en22016

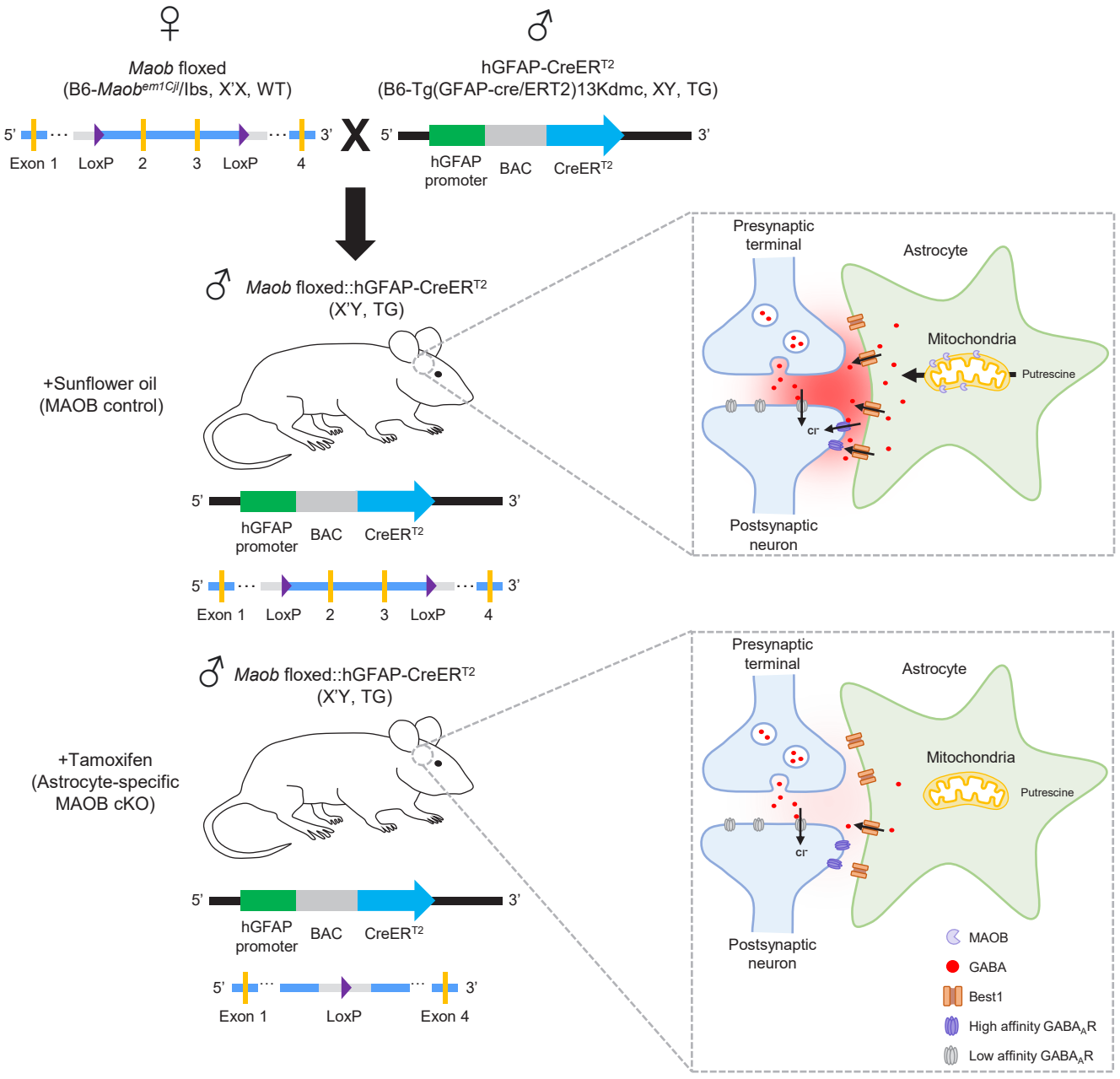

Fig. 6. Schematic illustration of generation (left) and characterization (right) of astrocyte-specific MAOB cKO mice. Tamoxifen-injected astrocyte-specific MAOB cKO mice show minimal tonic GABA inhibition with reduced levels of MAOB expression and GABA content in astrocytes, compared to sunflower oil-injected MAOB control mice.

exact role of astrocytic MAOB in the brain, because these mice do not express MAOB throughout the body from the developmental stage. Thus, another enzyme, diamine oxidase (DAO), as an alternative GABA-synthesizing enzyme [13, 34], might be recruited to compensate for MAOB deficiencies. Therefore, DAO elevation by compensatory mechanisms could lead to the synthesis of GABA from putrescine, resulting in a relapse of GABA production in MAOB null KO mice. In terms of tonic inhibition, astrocyte-specific MAOB cKO mice showed a 74.6% reduction in tonic GABA currents from granule cells in the cerebellum (Fig. 3C) and a 76.8% reduction from MSNs in the striatum (Fig. 5C), while MAOB null KO showed 60~65% and 50~55% reduction, respectively [9]. Therefore, compensatory mechanisms might explain the greater reduction in tonic inhibition in astrocyte-specific MAOB cKO than in MAOB null KO mice [9]. In addition, other studies have reported that developmental adaptations during brain maturation

in MAOB null KO mice may result in a phenotype different from that elicited by acute pharmacological intervention in adult WT mice [35]. Such a paradoxical finding might be the result of developmental compensation in MAOB null KO mice. The problem of turning on compensatory mechanisms can be circumvented by using our new mouse model, with temporal and regional (cell type-specific) control of MAOB ablation. Thus, future behavioral experiments, such as motor coordination [10] and anxiety-like behavior [35], are needed to determine the role of astrocytic MAOB and GABA in behavior and cognition using this new mouse model. In addition, we have previously reported that the astrocytic GABA exerts an inhibitory effect on the neuronal excitability of granule cells in the cerebellum [10] and dentate gyrus neurons in the hippocampus [12]. Therefore, it will be of great interest to examine whether astrocyte-specific MAOB cKO mice show altered spike probability and synaptic plasticity in the future investigation.

We have previously reported the astrocyte specificity of hGFAP-CreER^{T2} mouse line in several brain regions, by crossing this mouse line with Ai14 (RCL-tdTomato) and quantifying the proportion of co-labeled S100β- and tdTomato-positive cells in the total number of S100β-positive cells [25]. In this report, hGFAP-CreER^{T2} showed about 90% astrocyte specificity in the cerebellum and striatum [25], indicating that hGFAP-CreER^{T2} can be utilized to manipulate the gene of interest selectively expressed in astrocytes. Therefore, minimal tonic GABA inhibition in the cerebellum and striatum of astrocyte-specific MAOB cKO mice (Figs. 2~5) is mainly due to astrocytic MAOB ablation without neuronal effect. Although astrocytic MAOB ablation markedly reduced tonic inhibition, we observed some amount of remaining GABA immunoreactivity and about 25% of remaining tonic GABA current in astrocyte-specific MAOB cKO mice (Figs. 2~5). The remaining GABA might be synthesized by endogenous DAO as an alternative GABA-synthesizing enzyme [34].

In summary, we generated a new astrocyte-specific MAOB cKO mouse line with minimal tonic GABA inhibition, which can substitute for the MAOB null KO mice to investigate the role of cell type-specific MAOB in the brain. We expect that this new mouse model will be used extensively in various neurodegenerative and neurological diseases to improve understanding of the pathophysiological roles of astrocytic MAOB.

ACKNOWLEDGEMENTS

This work was supported by the Institute for Basic Science (IBS), Center for Cognition and Sociality (IBS-R001-D2) to C.J.L.

REFERENCES

1. Gorkin VZ. (1959) [On certain properties of monoaminoxidase in liver and brain mitochondria in rats]. Biokhimiia 24:826-832. Russian.
2. Tong J, Meyer JH, Furukawa Y, Boileau I, Chang LJ, Wilson AA, Houle S, Kish SJ (2013) Distribution of monoamine oxidase proteins in human brain: implications for brain imaging studies. J Cereb Blood Flow Metab 33:863-871.
3. Vitalis T, Fouquet C, Alvarez C, Seif I, Price D, Gaspar P, Cases O (2002) Developmental expression of monoamine oxidases A and B in the central and peripheral nervous systems of the mouse. J Comp Neurol 442:331-347.
4. Nam MH, Sa M, Ju YH, Park MG, Lee CJ (2022) Revisiting the role of astrocytic MAOB in Parkinson's disease. Int J Mol Sci 23:4453.
5. Fagervall I, Ross SB (1986) A and B forms of monoamine oxidase within the monoaminergic neurons of the rat brain. J Neurochem 47:569-576.
6. Thorpe LW, Westlund KN, Kochersperger LM, Abell CW, Denney RM (1987) Immunocytochemical localization of monoamine oxidases A and B in human peripheral tissues and brain. J Histochem Cytochem 35:23-32.
7. Levitt P, Pintar JE, Breakefield XO (1982) Immunocytochemical demonstration of monoamine oxidase B in brain astrocytes and serotonergic neurons. Proc Natl Acad Sci U S A 79:6385-6389.
8. Cho HU, Kim S, Sim J, Yang S, An H, Nam MH, Jang DP, Lee CJ (2021) Redefining differential roles of MAO-A in dopamine degradation and MAO-B in tonic GABA synthesis. Exp Mol Med 53:1148-1158.
9. Yoon BE, Woo J, Chun YE, Chun H, Jo S, Bae JY, An H, Min JO, Oh SJ, Han KS, Kim HY, Kim T, Kim YS, Bae YC, Lee CJ (2014) Glial GABA, synthesized by monoamine oxidase B, mediates tonic inhibition. J Physiol 592:4951-4968.
10. Woo J, Min JO, Kang DS, Kim YS, Jung GH, Park HJ, Kim S, An H, Kwon J, Kim J, Shim I, Kim HG, Lee CJ, Yoon BE (2018) Control of motor coordination by astrocytic tonic GABA release through modulation of excitation/inhibition balance in cerebellum. Proc Natl Acad Sci U S A 115:5004-5009.
11. Lee S, Yoon BE, Berglund K, Oh SJ, Park H, Shin HS, Augustine GJ, Lee CJ (2010) Channel-mediated tonic GABA release from glia. Science 330:790-796.
12. Jo S, Yarishkin O, Hwang YJ, Chun YE, Park M, Woo DH, Bae JY, Kim T, Lee J, Chun H, Park HJ, Lee DY, Hong J, Kim HY, Oh SJ, Park SJ, Lee H, Yoon BE, Kim Y, Jeong Y, Shim I, Bae YC, Cho J, Kowall NW, Ryu H, Hwang E, Kim D, Lee CJ (2014)

GABA from reactive astrocytes impairs memory in mouse models of Alzheimer's disease. Nat Med 20:886-896.
13. Park JH, Ju YH, Choi JW, Song HJ, Jang BK, Woo J, Chun H, Kim HJ, Shin SJ, Yarishkin O, Jo S, Park M, Yeon SK, Kim S, Kim J, Nam MH, Londhe AM, Kim J, Cho SJ, Cho S, Lee C, Hwang SY, Kim SW, Oh SJ, Cho J, Pae AN, Lee CJ, Park KD (2019) Newly developed reversible MAO-B inhibitor circumvents the shortcomings of irreversible inhibitors in Alzheimer's disease. Sci Adv 5:eaav0316.
14. Mallajosyula JK, Kaur D, Chinta SJ, Rajagopalan S, Rane A, Nicholls DG, Di Monte DA, Macarthur H, Andersen JK (2008) MAO-B elevation in mouse brain astrocytes results in Parkinson's pathology. PLoS One 3:e1616.
15. An H, Heo JY, Lee CJ, Nam MH (2021) The pathological role of astrocytic MAOB in Parkinsonism revealed by genetic ablation and over-expression of MAOB. Exp Neurobiol 30:113-119.
16. Nam MH, Cho J, Kwon DH, Park JY, Woo J, Lee JM, Lee S, Ko HY, Won W, Kim RG, Song H, Oh SJ, Choi JW, Park KD, Park EK, Jung H, Kim HS, Lee MC, Yun M, Lee CJ, Kim HI (2020) Excessive astrocytic GABA causes cortical hypometabolism and impedes functional recovery after subcortical stroke. Cell Rep 32:107861.
17. Chun H, Lim J, Park KD, Lee CJ (2022) Inhibition of monoamine oxidase B prevents reactive astrogliosis and scar formation in stab wound injury model. Glia 70:354-367.
18. Sa M, Yoo ES, Koh W, Park MG, Jang HJ, Yang YR, Lim J, Won W, Kwon J, Bhalla M, An H, Seong Y, Lee SE, Park KD, Suh PG, Sohn JW, Lee CJ (2022) Hypothalamic GABRA5-positive neurons control obesity via astrocytic GABA. bioRxiv. doi: 10.1101/2021.11.07.467613.
19. Richards G, Messer J, Waldvogel HJ, Gibbons HM, Dragunow M, Faull RL, Saura J (2011) Up-regulation of the isoenzymes MAO-A and MAO-B in the human basal ganglia and pons in Huntington's disease revealed by quantitative enzyme radioautography. Brain Res 1370:204-214.
20. Nishizono H, Hayano Y, Nakahata Y, Ishigaki Y, Yasuda R (2021) Rapid generation of conditional knockout mice using the CRISPR-Cas9 system and electroporation for neuroscience research. Mol Brain 14:148.
21. Capecchi MR (2005) Gene targeting in mice: functional analysis of the mammalian genome for the twenty-first century. Nat Rev Genet 6:507-512.
22. Cohen J (2016) 'Any idiot can do it.' Genome editor CRISPR could put mutant mice in everyone's reach. Science. doi: 10.1126/science.aal0334.
23. Wang H, Yang H, Shivalila CS, Dawlaty MM, Cheng AW, Zhang F, Jaenisch R (2013) One-step generation of mice carrying mutations in multiple genes by CRISPR/Cas-mediated genome engineering. Cell 153:910-918.
24. Yang H, Wang H, Shivalila CS, Cheng AW, Shi L, Jaenisch R (2013) One-step generation of mice carrying reporter and conditional alleles by CRISPR/Cas-mediated genome engineering. Cell 154:1370-1379.
25. Park YM, Chun H, Shin JI, Lee CJ (2018) Astrocyte specificity and coverage of hGFAP-CreERT2 [Tg(GFAP-Cre/ERT2)13Kdmc] mouse line in various brain regions. Exp Neurobiol 27:508-525.
26. Casper KB, Jones K, McCarthy KD (2007) Characterization of astrocyte-specific conditional knockouts. Genesis 45:292-299.
27. Srinivasan R, Lu TY, Chai H, Xu J, Huang BS, Golshani P, Coppola G, Khakh BS (2016) New transgenic mouse lines for selectively targeting astrocytes and studying calcium signals in astrocyte processes in situ and in vivo. Neuron 92:1181-1195.
28. Petryszak R, Keays M, Tang YA, Fonseca NA, Barrera E, Burdett T, Füllgrabe A, Fuentes AM, Jupp S, Koskinen S, Mannion O, Huerta L, Megy K, Snow C, Williams E, Barzine M, Hastings E, Weisser H, Wright J, Jaiswal P, Huber W, Choudhary J, Parkinson HE, Brazma A (2016) Expression atlas update--an integrated database of gene and protein expression in humans, animals and plants. Nucleic Acids Res 44:D746-D752.
29. An H, Koh W, Kang S, Nam MH, Lee CJ (2021) Differential proximity of perisynaptic astrocytic best1 at the excitatory and inhibitory tripartite synapses in APP/PS1 and MAOB-KO mice revealed by lattice structured illumination microscopy. Exp Neurobiol 30:213-221.
30. Kim YS, Woo J, Lee CJ, Yoon BE (2017) Decreased glial GABA and tonic inhibition in cerebellum of mouse model for attention-deficit/hyperactivity disorder (ADHD). Exp Neurobiol 26:206-212.
31. Ade KK, Janssen MJ, Ortinski PI, Vicini S (2008) Differential tonic GABA conductances in striatal medium spiny neurons. J Neurosci 28:1185-1197.
32. Maguire EP, Macpherson T, Swinny JD, Dixon CI, Herd MB, Belelli D, Stephens DN, King SL, Lambert JJ (2014) Tonic inhibition of accumbal spiny neurons by extrasynaptic α4βδ GABAA receptors modulates the actions of psychostimulants. J Neurosci 34:823-838.
33. Cahoy JD, Emery B, Kaushal A, Foo LC, Zamanian JL, Christopherson KS, Xing Y, Lubischer JL, Krieg PA, Krupenko SA, Thompson WJ, Barres BA (2008) A transcriptome database for astrocytes, neurons, and oligodendrocytes: a new resource

for understanding brain development and function. J Neurosci 28:264-278.

34. Kwak H, Koh W, Kim S, Song K, Shin JI, Lee JM, Lee EH, Bae JY, Ha GE, Oh JE, Park YM, Kim S, Feng J, Lee SE, Choi JW, Kim KH, Kim YS, Woo J, Lee D, Son T, Kwon SW, Park KD, Yoon BE, Lee J, Li Y, Lee H, Bae YC, Lee CJ, Cheong E (2020) Astrocytes control sensory acuity via tonic inhibition in the thalamus. Neuron 108:691-706.e10.

35. Chen K, Holschneider DP, Wu W, Rebrin I, Shih JC (2004) A spontaneous point mutation produces monoamine oxidase A/B knock-out mice with greatly elevated monoamines and anxiety-like behavior. J Biol Chem 279:39645-39652.

https://doi.org/10.5607/en22016